Frontiers of Information Technology & Electronic Engineering
www.jzus.zju.edu.cn; engineering.cae.cn; www.springerlink.com
ISSN 2095-9184 (print); ISSN 2095-9230 (online)
E-mail: jzus@zju.edu.cn

Smooth tracking control for conversion mode of a tilt-rotor aircraft with switching modeling*

Kebi LUO, Shuang SHI†‡, Cong PENG

College of Automation Engineering, Nanjing University of Aeronautics and Astronautics, Nanjing 211106, China

†E-mail: shishuang@nuaa.edu.cn

Received Apr. 13, 2023; Revision accepted July 6, 2023; Crosschecked Oct. 25, 2023

Abstract: This paper investigates the state-tracking control problem in conversion mode of a tilt-rotor aircraft with a switching modeling method and a smooth interpolation technique. Based on the nonlinear model of the conversion mode, a switched linear model is developed by using the Jacobian linearization method and designing the switching signal based on the mast angle. Furthermore, an $\mathcal{H}_\infty$ state-tracking control scheme is designed to deal with the conversion mode control issue. Moreover, instead of limiting the amplitude of control inputs, a smooth interpolation method is developed to create bumpless performance. Finally, the XV-15 tilt-rotor aircraft is chosen as a prototype to illustrate the effectiveness of this developed control method.

Key words: Tilt-rotor aircraft; State-tracking control; Switched linear systems; Time-scheduled multiple Lyapunov function approach; Smooth interpolation

https://doi.org/10.1631/FITEE.2300266 **CLC number:** TP18; V279

1 Introduction

A tilt-rotor aircraft can switch between helicopter mode and airplane mode by installing two rotating nacelles to the tips of wings, which has the advantages of both fixed-wing aircrafts and helicopters (Thompson, 1990). The mode in which a tilt-rotor aircraft transforms between these two modes is called conversion mode, and it includes the characteristics of full flight modes (Rysdyk RT and Calise, 1999). Modeling a tilt-rotor aircraft in conversion mode is arduous, because it is difficult to reconcile the accuracy of the mathematical model and the difficulty of control design. For instance, a simplified nonlinear mathematical model was built based on the Euler equations in Kleinhesselink (2007). However, this simplified model is inaccurate because of the rotor effects. Simplifying the model can make the control design easier, but the model might be inaccurate. Designing control laws based on a nonlinear model is also a challenge, due to complex changes in dynamic characteristics and other problems (Rysdyk R and Calise, 2005). Although the transition process lasts only for a couple of seconds, it is still the most complicated and significant part (Li Z and Xia, 2018). Consequently, many scholars have focused on the modeling and control issues of conversion mode (Wang YE et al., 2016; Barra et al., 2019; Abà et al., 2020).

The aerodynamic features change violently as the nacelles tilt. Thus, it is difficult to describe the transition process with a single mathematical model. It is also difficult to design control schemes directly for nonlinear models (Chen et al., 2017; Li YL et al., 2022; Tang et al., 2022; Zhao H et al., 2023). Modeling by the switched system and designing the switching control scheme can effectively

‡ Corresponding author

* Project supported by the National Natural Science Foundation of China (Nos. 62103186 and 62122038), the Natural Science Foundation of Jiangsu Province, China (Nos. BK20210285 and BK20211565), and the China Postdoctoral Science Foundation (Nos. 2021TQ0151 and 2021M691571)

ORCID: Kebi LUO, https://orcid.org/0009-0001-3719-4086; Shuang SHI, https://orcid.org/0000-0001-6000-0350

resolve this problem. In Wang XH and Cai (2015), a switching control method was adopted in controller design based on a nonlinear model of conversion mode. A novel tilt-rotor was studied in Kong and Lu (2018), and a switching control law was designed by developing the back-stepping method. However, the tilting features were eliminated in designing the back-stepping controller. The methods above apply switching method to complete the switching controller design, but the nonlinear aerodynamic model is adopted for the modeling. A switched system generally consists of a number of subsystems and a switching law representing the switching order (Zhao XD et al., 2012; Ye et al., 2021; Hou et al., 2022; Roy et al., 2022). Modeling the tilting process by a switched linear model can obtain more tilting features, and the violent changes of aerodynamic parameters can be depicted more precisely. Moreover, the control design can be simplified based on the switched linear model.

Due to the switching characteristic, abrupt controller bumps will appear when switching occurs at the switching instants, which may destroy the performance and even the stability of the system. To reduce controller bumps, a bumpless transfer method is necessary to make the control input smooth at switching instants, which can further improve the transient performance of the system. In Daafouz et al. (2012), an additional global condition was introduced to restrain the controller gain. However, finding a feasible solution to avoid this global limitation is difficult (Yang and Zhao, 2019). To release this constraint, a local condition was proposed instead, and this bumpless transfer method was widely used (Yang and Zhao, 2019; Zhao Y and Zhao, 2020; Zhao Y et al., 2020). This approach requires a reference input to limit the amplitude range of the actual control input. As a result, the disparity of the control signal between adjacent sides of a switching instant can be maintained at a small level. Unfortunately, there is still no effective way to obtain a proper reference input.

An admissible solution to the previous problem is to develop a bumpless control architecture without reference control inputs. Recently, the time-scheduled multiple Lyapunov function (MLF) approach was exploited for analysis and synthesis of switched systems, which can achieve better performance than traditional time-independent MLF methods (Allerhand and Shaked, 2011; Xiang, 2015; Yuan et al., 2018; Shi et al., 2021; Fei et al., 2023). However, the time-scheduled MLF is discontinuous at switching instants, which leads to controller bumps. In this paper, the time-scheduled method is further developed to construct an improved MLF. An additional subinterval is introduced after each switching (called a transition interval), and the linear interpolation method is adopted in transition intervals. By this manipulation, the revised MLF is continuous and non-increasing at the switching instants. Accordingly, the designed control scheme can decrease controller bumps without introducing an additional reference input.

In this paper, the conversion mode of a tilt-rotor aircraft is built as a switched linear system. On this foundation, an improved time-scheduled MLF technique is proposed to develop a smooth $\mathcal{H}_\infty$ state-tracking control scheme, which can accomplish a smooth transition between helicopter mode and airplane mode. The main improvements of this article are twofold:

1. A switched linear model of a tilt-rotor aircraft in conversion mode is built. As a result, the nonlinear control problem of the conversion mode is transformed into the state-tracking control issue of the switched linear system.

2. A time-scheduled method is developed to construct an improved MLF. On this basis, the linear interpolation method is adopted in transition intervals to resolve the bumpless transfer issue. Compared with the conventional bumpless transfer technique, the reference input is no longer essential.

2 Switching modeling for the longitudinal dynamic model of a tilt-rotor aircraft

The partonomy is used in the modeling process, and the model is simplified into a longitudinal dynamic model. Some assumptions are essential in the modeling process (Harendra et al., 1973). For instance, each component of a tilt-rotor aircraft is rigid body and the rotation speed of the rotor is regarded as fixed during the process.

Take the XV-15 tilt-rotor aircraft as an example. Based on the Euler equations (Kleinhesselink, 2007), the longitudinal dynamic model for conversion mode

is

$$\begin{cases} m_g\dot{u} = -m_g wq - m_g g\sin\theta + F_x, \\ m_g\dot{w} = m_g uq + m_g g\cos\theta + F_z, \\ I_y\dot{q} = M_y, \\ \dot{\theta} = q, \end{cases} \tag{1}$$

where u, w, q, and θ denote the forward speed, longitudinal speed, pitch rate, and pitch angle, respectively. m_g is the mass of the aircraft, g is the gravitational acceleration, and I_y is the pitch rotational inertia. F_x denotes the resultant aerodynamic force of each part in the x direction, while F_z denotes the force in the z direction. M_y represents the resultant aerodynamic moment of each component in the y direction. These forces and moments are related to the collective pitch $\theta_{\rm b}$, the longitudinal periodic pitch $\theta_{\rm a}$, the elevator deflection $\delta_{\rm e}$, and the mast angle $\beta_{\rm M}$.

Maisel et al. (2000) presented the conversion corridor with respect to the mast angle $\beta_{\rm M}$ and the air speed V, which can guarantee a safe tilting process. By selecting N operating points in the conversion corridor, trimming the nonlinear model of conversion mode (1), and taking the Jacobian linearization, a cluster of linear models are obtained. Furthermore, introducing a switching signal $\sigma(t)$, nonlinear model (1) can be transformed to a switched linear system:

$$\dot{\boldsymbol{x}}(t) = \boldsymbol{A}_{\sigma(t)}\boldsymbol{x}(t) + \boldsymbol{B}_{\sigma(t)}\boldsymbol{u}(t) + \boldsymbol{H}_{\sigma(t)}\boldsymbol{\omega}(t), \tag{2}$$

where $\boldsymbol{x}(t) = [\Delta u, \Delta w, \Delta q, \Delta\theta]^{\rm T}$ is the state, $\boldsymbol{u}(t) = [\Delta\theta_{\rm b}, \Delta\theta_{\rm a}, \Delta\delta_{\rm e}]^{\rm T}$ is the input, and $\boldsymbol{\omega}(t)$ is the external disturbance. $\sigma(t) : [0,\infty) \to \mathcal{R}_N \triangleq \{1, 2, \cdots, N\}$ is the switching signal. $\boldsymbol{A}_i$, $\boldsymbol{B}_i$, and $\boldsymbol{H}_i$ ($\sigma(t) = i,\ i \in \mathcal{R}_N$) are matrices with proper dimensions, and these matrix parameters are derived based on the trimming results.

Definition 1 (Zhao XD et al., 2012) The switching law $\sigma(t) = i,\ i \in \mathcal{R}_N$, can be called mode-dependent dwell-time (MDDT) switching if

$$N_i(t_x, t_y) \le 1 + T_i(t_x, t_y)/\tau_{{\rm d}i},\ \ \forall t_y > t_x \ge 0,$$

where $\tau_{{\rm d}i} > 0$ is an existing scalar, $N_i(t_x, t_y)$ and $T_i(t_x, t_y)$ represent the overall number that switches to the $i^{\rm th}$ mode and the total activated time of the $i^{\rm th}$ subsystem ($i \in \mathcal{R}_N$) in the interval $[t_x, t_y)$, respectively. Then, $\tau_{{\rm d}i}$ is called MDDT.

Remark 1 The mast angle $\beta_{\rm M}$ is closely related to the inclination angle of the nacelles. In conversion mode, the variation of $\beta_{\rm M}$ from 0° to 90° represents the flight mode of the tilt-rotor aircraft changing from helicopter mode to airplane mode. By linearizing nonlinear model (1) based on the range of $\beta_{\rm M}$, the switched linear system (2) is obtained, and thus the runtime of each subsystem in Eq. (2) has a lower bound. This MDDT switching can further describe the tilting characteristics.

3 Smooth $\mathcal{H}_\infty$ state-tracking control

In this section, the interval partitioning and smooth interpolation methods are further extended to develop an improved MLF. On this basis, an $\mathcal{H}_\infty$ state-tracking control scheme is proposed for the switched linear system (2).

The reference model can be scrupulously extracted from the tilting course based on the state characteristics and trimming results:

$$\dot{\boldsymbol{x}}_{\rm r}(t) = \boldsymbol{A}_{\rm r}\boldsymbol{x}_{\rm r}(t) + \boldsymbol{B}_{\rm r}\boldsymbol{r}(t), \tag{3}$$

where $\boldsymbol{x}_{\rm r}(t) \in \mathbb{R}^{n_x}$ and $\boldsymbol{r}(t) \in \mathbb{R}^{n_r}$ represent the state and input of the reference system, respectively. This reference system generates desirable state trajectories to be tracked. To ensure favorable tracking performance, $\boldsymbol{A}_{\rm r}$ should have the same matrix structure as $\boldsymbol{A}_i$, $i \in \mathcal{R}_N$.

Considering the switched system (2) with reference model (3), define the tracking error as $\boldsymbol{e}(t) = \boldsymbol{x}(t) - \boldsymbol{x}_{\rm r}(t)$. The control input is designed as

$$\boldsymbol{u}(t) = \boldsymbol{K}_{{\rm e}i}(t)\boldsymbol{e}(t) + \boldsymbol{K}_{{\rm c}i}\boldsymbol{x}_{\rm r}(t) + \boldsymbol{K}_{{\rm r}i}\boldsymbol{r}(t), \tag{4}$$

where $\boldsymbol{K}_{{\rm e}i}(t)$, $\boldsymbol{K}_{{\rm c}i}$, and $\boldsymbol{K}_{{\rm r}i}$ are controller gain matrices, $i \in \mathcal{R}_N$. One can further deduce that

$$\dot{\boldsymbol{e}}(t) = \boldsymbol{\Lambda}_{{\rm e}i}\boldsymbol{e}(t) + \boldsymbol{\Lambda}_{{\rm c}i}\boldsymbol{x}_{\rm r}(t) + \boldsymbol{\Lambda}_{{\rm r}i}\boldsymbol{r}(t) + \boldsymbol{H}_i\boldsymbol{\omega}(t), \tag{5}$$

where $\boldsymbol{\Lambda}_{{\rm e}i} = \boldsymbol{A}_i + \boldsymbol{B}_i\boldsymbol{K}_{{\rm e}i}(t)$, $\boldsymbol{\Lambda}_{{\rm c}i} = \boldsymbol{A}_i + \boldsymbol{B}_i\boldsymbol{K}_{{\rm c}i} - \boldsymbol{A}_{\rm r}$, and $\boldsymbol{\Lambda}_{{\rm r}i} = \boldsymbol{B}_i\boldsymbol{K}_{{\rm r}i} - \boldsymbol{B}_{\rm r}$, $\forall\sigma(t) = i,\ i \in \mathcal{R}_N$. Select $\boldsymbol{K}_{{\rm c}i}$ and $\boldsymbol{K}_{{\rm r}i}$ such that $\boldsymbol{\Lambda}_{{\rm c}i} = \boldsymbol{0}$ and $\boldsymbol{\Lambda}_{{\rm r}i} = \boldsymbol{0}$. Hence, the trajectory tracking issue becomes the stabilization issue of tracking error system (5).

Definition 2 Considering the switched system (2) with reference model (3), if there exist switching signal $\sigma(t)$ and controller (4) satisfying

(1) when $\boldsymbol{\omega}(t) \equiv \boldsymbol{0}$ and system (5) is globally uniformly exponentially stable (GUES),

$$\|\boldsymbol{e}(t)\| \le \nu\exp\big(\epsilon(t - t_0)\big)\|\boldsymbol{e}(t_0)\|,\ \ \forall t \ge t_0,$$

(2) when $\boldsymbol{\omega}(t) \neq \mathbf{0}$ and under the zero initial condition,

$$\int_0^\infty \boldsymbol{e}^{\mathrm{T}}(\vartheta)\boldsymbol{e}(\vartheta)\mathrm{d}\vartheta \leq \tilde{\gamma}^2 \int_0^\infty \boldsymbol{\omega}^{\mathrm{T}}(\vartheta)\boldsymbol{\omega}(\vartheta)\mathrm{d}\vartheta,$$

where $\nu > 0$, $\epsilon > 0$, and $\tilde{\gamma} > 0$ are constants, then system (5) is said to achieve an $\mathcal{H}_\infty$ state-tracking performance.

The control objective here is to co-design controller (4) and an MDDT switching law such that tracking error system (5) has an $\mathcal{H}_\infty$ tracking performance.

Inspired by interpolation approaches in several works (Allerhand and Shaked, 2011; Xiang, 2015; Yuan et al., 2018), here we introduce a scalar τ_{h} and let $[t_s, t_s + \tau_{\mathrm{h}})$ denote the transition interval, where t_s denotes the s^{th} switching instant. The interpolation process is developed during the interval to design time-scheduled controllers, which can prevent abrupt bumps appearing at switching instants. Additionally, let the interval $[t_s + \tau_{\mathrm{h}}, t_{s+1})$ be partitioned into $L+1$ portions. Define a time sequence $\{t_{s0}, t_{s1}, \cdots, t_{sL}\}$, where $t_{s0} = t_s + \tau_{\mathrm{h}}$. Eventually, the interval $[t_s, t_{s+1})$ is divided into $[t_s, t_{s0}) \cup [t_{s0}, t_{s1}) \cup \cdots \cup [t_{s(L-1)}, t_{sL}) \cup [t_{sL}, t_{s+1})$. Let the length of each portion except $[t_{sL}, t_{s+1})$ be $\tau_{\mathrm{l}i}$ for $\sigma(t_s) = i$, $i \in \mathcal{R}_N$ and $l \in \mathbb{Z}_{[0,L]}$. To realize this partitioning approach, $\tau_{\mathrm{d}i} > \tau_{\mathrm{h}} + L\tau_{\mathrm{l}i}$ is obviously required for $i \in \mathcal{R}_N$. Based on such a partitioning, a smooth $\mathcal{H}_\infty$ state-tracking control scheme is developed.

Theorem 1 Consider the switched linear system (2) with reference model (3). Let $\varsigma_{\mathrm{s}i} \geq \varsigma_{\mathrm{u}i} > 0$, $\tau_{\mathrm{l}i} > 0$, $\tau_{\mathrm{h}} > 0$ be given constants for $i \in \mathcal{R}_N$, and $\gamma > 0$, and suppose that there exist matrices $\boldsymbol{T}_{ik} > 0$ and $\boldsymbol{U}_{ik}$ for $(i,j) \in \mathcal{R}_N \times \mathcal{R}_N$, $i \neq j$, $k \in \mathbb{Z}_{[0,L]}$, $l \in \mathbb{Z}_{[0,L-1]}$,

$$\tilde{\boldsymbol{\chi}}_{1ij} = \begin{bmatrix} \tilde{\boldsymbol{\chi}}_{1ij}^{11} & \boldsymbol{H}_i & \boldsymbol{T}_{jL} \\ * & -\gamma^2\boldsymbol{I} & \mathbf{0} \\ * & \mathbf{0} & -\boldsymbol{I} \end{bmatrix} < 0, \tag{6}$$

$$\tilde{\boldsymbol{\chi}}_{2ij} = \begin{bmatrix} \tilde{\boldsymbol{\chi}}_{2ij}^{11} & \boldsymbol{H}_i & \boldsymbol{T}_{i0} \\ * & -\gamma^2\boldsymbol{I} & \mathbf{0} \\ * & \mathbf{0} & -\boldsymbol{I} \end{bmatrix} < 0, \tag{7}$$

$$\bar{\boldsymbol{\chi}}_{1ij} = \begin{bmatrix} \bar{\boldsymbol{\chi}}_{1ij}^{11} & \boldsymbol{H}_i & \boldsymbol{T}_{il} \\ * & -\gamma^2\boldsymbol{I} & \mathbf{0} \\ * & \mathbf{0} & -\boldsymbol{I} \end{bmatrix} < 0, \tag{8}$$

$$\bar{\boldsymbol{\chi}}_{2ij} = \begin{bmatrix} \bar{\boldsymbol{\chi}}_{1ij}^{11} & \boldsymbol{H}_i & \boldsymbol{T}_{i(l+1)} \\ * & -\gamma^2\boldsymbol{I} & \mathbf{0} \\ * & \mathbf{0} & -\boldsymbol{I} \end{bmatrix} < 0, \tag{9}$$

$$\boldsymbol{\chi}_i = \begin{bmatrix} \boldsymbol{\chi}_i^{11} & \boldsymbol{H}_i & \boldsymbol{T}_{iL} \\ * & -\gamma^2\boldsymbol{I} & \mathbf{0} \\ * & \mathbf{0} & -\boldsymbol{I} \end{bmatrix} < 0, \tag{10}$$

where

$$\begin{aligned}
\tilde{\boldsymbol{\chi}}_{1ij}^{11} =& \mathrm{He}\{\boldsymbol{A}_i\boldsymbol{T}_{jL} + \boldsymbol{B}_i\boldsymbol{U}_{jL}\} + \varsigma_{\mathrm{u}i}\boldsymbol{T}_{jL} - \frac{\boldsymbol{T}_{i0} - \boldsymbol{T}_{jL}}{\tau_{\mathrm{h}}},\\
\tilde{\boldsymbol{\chi}}_{2ij}^{11} =& \mathrm{He}\{\boldsymbol{A}_i\boldsymbol{T}_{i0} + \boldsymbol{B}_i\boldsymbol{U}_{i0}\} + \varsigma_{\mathrm{u}i}\boldsymbol{T}_{i0} - \frac{\boldsymbol{T}_{i0} - \boldsymbol{T}_{jL}}{\tau_{\mathrm{h}}},\\
\bar{\boldsymbol{\chi}}_{1ij}^{11} =& \mathrm{He}\{\boldsymbol{A}_i\boldsymbol{T}_{il} + \boldsymbol{B}_i\boldsymbol{U}_{il}\} + \varsigma_{\mathrm{s}i}\boldsymbol{T}_{il} - \frac{\boldsymbol{T}_{i(l+1)} - \boldsymbol{T}_{il}}{\tau_{\mathrm{l}i}},\\
\bar{\boldsymbol{\chi}}_{2ij}^{11} =& \mathrm{He}\{\boldsymbol{A}_i\boldsymbol{T}_{i(l+1)} + \boldsymbol{B}_i\boldsymbol{U}_{i(l+1)}\} + \varsigma_{\mathrm{s}i}\boldsymbol{T}_{i(l+1)}\\
&- \frac{\boldsymbol{T}_{i(l+1)} - \boldsymbol{T}_{il}}{\tau_{\mathrm{l}i}},\\
\boldsymbol{\chi}_i^{11} =& \mathrm{He}\{\boldsymbol{A}_i\boldsymbol{T}_{iL} + \boldsymbol{B}_i\boldsymbol{U}_{iL}\} + \varsigma_{\mathrm{s}i}\boldsymbol{T}_{iL},
\end{aligned}$$

with $\mathrm{He}\{\boldsymbol{X}\} \triangleq \boldsymbol{X} + \boldsymbol{X}^{\mathrm{T}}$.

Then, for the MDDT switching signal satisfying $\tau_{\mathrm{d}i} > \tau_{\mathrm{h}} + L\tau_{\mathrm{l}i}$, $i \in \mathcal{R}_N$, the closed-loop system (5) has an $\mathcal{H}_\infty$ state-tracking performance no greater than

$$\tilde{\gamma} = \sqrt{\frac{\overline{\varsigma}_{\mathrm{s}}\alpha}{\underline{\varsigma}_{\mathrm{u}}}}\gamma, \tag{11}$$

where $\overline{\varsigma}_{\mathrm{s}} = \max_{i\in\mathcal{R}_N}(\varsigma_{\mathrm{s}i})$, $\underline{\varsigma}_{\mathrm{u}} = \min_{i\in\mathcal{R}_N}(\varsigma_{\mathrm{u}i})$, and $\alpha = \exp\big(\sum_{i\in\mathcal{R}_N}(\varsigma_{\mathrm{s}i} - \varsigma_{\mathrm{u}i})\tau_{\mathrm{h}}\big)$.

In addition, the controller gains in Eq. (4) satisfy $\boldsymbol{K}_{\mathrm{e}i}(t)\boldsymbol{T}_i(t) = \boldsymbol{U}_i(t)$, $\boldsymbol{A}_i + \boldsymbol{B}_i\boldsymbol{K}_{\mathrm{c}i} = \boldsymbol{A}_{\mathrm{r}}$, and $\boldsymbol{B}_i\boldsymbol{K}_{\mathrm{r}i} = \boldsymbol{B}_{\mathrm{r}}$, where for $(i,j) \in \mathcal{R}_N \times \mathcal{R}_N$, $i \neq j$, $l \in \mathbb{Z}_{[0,L-1]}$, $\sigma(0) = m \in \mathcal{R}_N$:

$$\boldsymbol{T}_i(t) = \begin{cases} \boldsymbol{T}_{jL} + \kappa(t)(\boldsymbol{T}_{i0} - \boldsymbol{T}_{jL}), & t \in [t_s, t_{s0}),\\ \boldsymbol{T}_{il} + \kappa_i(t)(\boldsymbol{T}_{i(l+1)} - \boldsymbol{T}_{il}), & t \in [t_{sl}, t_{s(l+1)}),\\ \boldsymbol{T}_{iL}, & t \in [t_{sL}, t_{s+1}),\\ \boldsymbol{T}_{mL}, & t \in [0, t_1), \end{cases} \tag{12}$$

$$\boldsymbol{U}_i(t) = \begin{cases} \boldsymbol{U}_{jL} + \kappa(t)(\boldsymbol{U}_{i0} - \boldsymbol{U}_{jL}), & t \in [t_s, t_{s0}),\\ \boldsymbol{U}_{il} + \kappa_i(t)(\boldsymbol{U}_{i(l+1)} - \boldsymbol{U}_{il}), & t \in [t_{sl}, t_{s(l+1)}),\\ \boldsymbol{U}_{iL}, & t \in [t_{sL}, t_{s+1}),\\ \boldsymbol{U}_{mL}, & t \in [0, t_1), \end{cases} \tag{13}$$

with $\kappa(t) = (t - t_s)/\tau_{\mathrm{h}}$ and $\kappa_i(t) = (t - t_{sl})/\tau_{\mathrm{l}i}$.

Proof Without loss of generality, consider $\sigma(t_s) = i$, $i \in \mathcal{R}_N$, and $\sigma(t_s^-) = j$, $j \in \mathcal{R}_N$, $i \neq j$.

Construct the following revised MLF:

$$V(\boldsymbol{e}(t)) = \boldsymbol{e}^{\mathrm{T}}(t)\boldsymbol{P}_i(t)\boldsymbol{e}(t), \tag{14}$$

where $\boldsymbol{P}_i(t)=\boldsymbol{T}_i^{-1}(t)$ for $t\in[0,\infty)$. It can be verified that the constructed Lyapunov function is continuous and differential for $t\in[0,\infty)$.

For $t\in[t_s,t_{s0})$, one can deduce that

$$\dot{V}(\boldsymbol{e}(t))+\boldsymbol{e}^{\mathrm{T}}(t)\boldsymbol{e}(t)-\gamma^2\boldsymbol{\omega}^{\mathrm{T}}(t)\boldsymbol{\omega}(t)=\boldsymbol{\zeta}^{\mathrm{T}}(t)\tilde{\boldsymbol{\Theta}}(t)\boldsymbol{\zeta}(t), \tag{15}$$

where $\boldsymbol{\zeta}(t)=\left[\begin{array}{cc}\boldsymbol{e}^{\mathrm{T}}(t) & \boldsymbol{\omega}^{\mathrm{T}}(t)\end{array}\right]^{\mathrm{T}}$, and

$$\tilde{\boldsymbol{\Theta}}(t)=\left[\begin{array}{cc}\tilde{\boldsymbol{\Theta}}^{11}(t) & \boldsymbol{P}_i(t)\boldsymbol{H}_i\\ * & -\gamma^2\boldsymbol{I}\end{array}\right]$$

with $\tilde{\boldsymbol{\Theta}}^{11}(t)=\mathrm{He}\{\boldsymbol{P}_i(t)\boldsymbol{A}_i+\boldsymbol{P}_i(t)\boldsymbol{B}_i\boldsymbol{K}_{\mathrm{e}i}(t)\}+\boldsymbol{I}+\dot{\boldsymbol{P}}_i(t)$.

In addition, define

$$\begin{aligned}\tilde{\boldsymbol{\chi}}_{ij}(t)=&(1-\kappa(t))\tilde{\boldsymbol{\chi}}_{1ij}(t)+\kappa(t)\tilde{\boldsymbol{\chi}}_{2ij}(t)\\=&\left[\begin{array}{ccc}\tilde{\boldsymbol{\chi}}_{ij}^{11}(t) & \boldsymbol{H}_i & \boldsymbol{T}_i\\ * & -\gamma^2\boldsymbol{I} & \boldsymbol{0}\\ * & \boldsymbol{0} & -\boldsymbol{I}\end{array}\right]\end{aligned}$$

with $\tilde{\boldsymbol{\chi}}_{ij}^{11}(t)=\mathrm{He}\{\boldsymbol{A}_i\boldsymbol{T}_i(t)+\boldsymbol{B}_i\boldsymbol{U}_i(t)\}+\varsigma_{\mathrm{u}i}\boldsymbol{T}_i(t)-\dot{\boldsymbol{T}}_i(t)$. It is noted that $0\le\kappa(t)<1$ for $t\in[t_s,t_{s0})$. According to inequalities (6) and (7) and Eqs. (12) and (13), one can deduce that $\tilde{\boldsymbol{\chi}}_{ij}(t)<0$.

Pre- and post-multiplying $\tilde{\boldsymbol{\chi}}_{ij}(t)$ by $\mathrm{diag}\{\boldsymbol{P}_i(t),\boldsymbol{I},\boldsymbol{I}\}$, one can obtain that

$$\left[\begin{array}{ccc}\boldsymbol{\chi}_{ij}^{11}(t) & \boldsymbol{P}_i(t)\boldsymbol{H}_i & \boldsymbol{I}\\ * & -\gamma^2\boldsymbol{I} & \boldsymbol{0}\\ * & \boldsymbol{0} & -\boldsymbol{I}\end{array}\right]<0$$

with $\boldsymbol{\chi}_{ij}^{11}(t)=\mathrm{He}\{\boldsymbol{P}_i(t)\boldsymbol{A}_i+\boldsymbol{P}_i(t)\boldsymbol{B}_i\boldsymbol{K}_{\mathrm{e}i}(t)\}+\varsigma_{\mathrm{u}i}\boldsymbol{P}_i(t)+\dot{\boldsymbol{P}}_i(t)$. Applying the Schur complement, $\tilde{\boldsymbol{\Theta}}(t)<0$ can be deduced. Combining with Eq. (15), one can further deduce that

$$\dot{V}(\boldsymbol{e}(t))+\boldsymbol{e}^{\mathrm{T}}(t)\boldsymbol{e}(t)-\gamma^2\boldsymbol{\omega}^{\mathrm{T}}(t)\boldsymbol{\omega}(t)<-\varsigma_{\mathrm{u}i}V(\boldsymbol{e}(t)). \tag{16}$$

By similar manipulation, for $t\in[t_{sl},t_{s(l+1)})$, $l\in\mathbb{Z}_{[0,L-1]}$,

$$\dot{V}(\boldsymbol{e}(t))+\boldsymbol{e}^{\mathrm{T}}(t)\boldsymbol{e}(t)-\gamma^2\boldsymbol{\omega}^{\mathrm{T}}(t)\boldsymbol{\omega}(t)<-\varsigma_{\mathrm{s}i}V(\boldsymbol{e}(t)) \tag{17}$$

can be guaranteed by inequalities (8) and (9). Meanwhile, inequality (10) can guarantee inequality (17) for $t\in[t_{sL},t_{s+1})$.

First, consider $\boldsymbol{\omega}(t)\equiv\boldsymbol{0}$. By integrating inequalities (16) and (17) from t_s to t_{s+1}, one can obtain that

$$\begin{aligned}&V(\boldsymbol{e}(t))\\\le&\exp\big\{-\varsigma_{\mathrm{u}i(t_s)}\tau_{\mathrm{h}}-\varsigma_{\mathrm{s}i(t_s)}(t-t_s-\tau_{\mathrm{h}})\big\}V(\boldsymbol{e}(t_s))\\\le&\prod_{i\in\mathcal{R}_N}\exp\big\{\varsigma_i\tau_{\mathrm{h}}N_i(t_0,t)-\varsigma_{\mathrm{s}i}T_i(t_0,t)\big\}V(\boldsymbol{e}(t_0))\\\le&\alpha\exp\Big\{\sum_{i\in\mathcal{R}_N}\big(\frac{\varsigma_i\tau_{\mathrm{h}}}{\tau_{\mathrm{d}i}}-\varsigma_{\mathrm{s}i}\big)T_i(t_0,t)\Big\}V(\boldsymbol{e}(t_0)),\end{aligned}$$

where $\varsigma_i=\varsigma_{\mathrm{s}i}-\varsigma_{\mathrm{u}i}$ for $i\in\mathcal{R}_N$. Because $\tau_{\mathrm{d}i}>\tau_{\mathrm{h}}$, one can deduce that $V(\boldsymbol{e}(t))\le\alpha\exp(-\underline{\varsigma}_{\mathrm{u}}(t-t_0))V(\boldsymbol{e}(t_0))$, where $\underline{\varsigma}_{\mathrm{u}}=\min_{i\in\mathcal{R}_N}(\varsigma_{\mathrm{u}i})$ as mentioned. Furthermore, it is observed that $V(\boldsymbol{e}(t))$ converges to 0 as $t\to\infty$. Then one can deduce that the system is GUES.

Next, consider $\boldsymbol{\omega}(t)\neq\boldsymbol{0}$. Integrating inequalities (16) and (17) from t_s to t_{s+1} and letting $\boldsymbol{F}(t)=\boldsymbol{e}^{\mathrm{T}}(t)\boldsymbol{e}(t)-\gamma^2\boldsymbol{\omega}^{\mathrm{T}}(t)\boldsymbol{\omega}(t)$, it holds that

$$\begin{aligned}&V(\boldsymbol{e}(t))\\\le&\exp\big\{-\varsigma_{\mathrm{u}i(t_s)}\tau_{\mathrm{h}}-\varsigma_{\mathrm{s}i(t_s)}(t-t_s-\tau_{\mathrm{h}})\big\}V(\boldsymbol{e}(t_s))\\&-\int_{t_s}^{t}\exp\big\{\varsigma_{\mathrm{u}i(t_s)}T_{\mathrm{h}i}(\vartheta,t)-\varsigma_{\mathrm{s}i(t_s)}T_i(\vartheta,t)\big\}\boldsymbol{F}(\vartheta)\mathrm{d}\vartheta\\\le&\prod_{i\in\mathcal{R}_N}\exp\big\{\varsigma_i\tau_{\mathrm{h}}N_i(t_0,t)-\varsigma_{\mathrm{s}i}T_i(t_0,t)\big\}V(\boldsymbol{e}(t_0))\\&-\int_{t_0}^{t}\prod_{i\in\mathcal{R}_N}\exp\big\{\varsigma_iT_{\mathrm{h}i}(\vartheta,t)-\varsigma_{\mathrm{s}i}T_i(\vartheta,t)\big\}\boldsymbol{F}(\vartheta)\mathrm{d}\vartheta,\end{aligned}$$

where $T_{\mathrm{h}i}(\vartheta,t)$ denotes the total length of transition intervals during $[\vartheta,t)$ of the i^{th} subsystem for $i\in\mathcal{R}_N$. It holds that $T_{\mathrm{h}i}(\vartheta,t)\le\tau_{\mathrm{h}}N_i(\vartheta,t)$.

Consider the zero initial condition. Because $V(\boldsymbol{e}(t))\ge0$, one can deduce that

$$\begin{aligned}&\int_{t_0}^{t}\prod_{i\in\mathcal{R}_N}\exp\big\{\varsigma_{i(t_s)}T_{\mathrm{h}i}(\vartheta,t)-\varsigma_{\mathrm{s}i(t_s)}T_i(\vartheta,t)\big\}\|\boldsymbol{e}(\vartheta)\|^2\mathrm{d}\vartheta\\\le&\int_{t_0}^{t}\prod_{i\in\mathcal{R}_N}\exp\big\{\varsigma_{i(t_s)}T_{\mathrm{h}i}(\vartheta,t)-\varsigma_{\mathrm{s}i(t_s)}T_i(\vartheta,t)\big\}\gamma^2\|\boldsymbol{\omega}(\vartheta)\|^2\mathrm{d}\vartheta.\end{aligned} \tag{18}$$

The left-hand side of inequality (18) satisfies

$$\begin{aligned}&\int_{t_0}^{t}\prod_{i\in\mathcal{R}_N}\exp\big\{\varsigma_{i(t_s)}T_{\mathrm{h}i}(\vartheta,t)-\varsigma_{\mathrm{s}i(t_s)}T_i(\vartheta,t)\big\}\|\boldsymbol{e}(\vartheta)\|^2\mathrm{d}\vartheta\\\ge&\int_{t_0}^{t}\exp\big\{-\overline{\varsigma}_{\mathrm{s}}(t-\vartheta)\big\}\|\boldsymbol{e}(\vartheta)\|^2\mathrm{d}\vartheta,\end{aligned} \tag{19}$$

while the right-hand side of inequality (18) satisfies

$$\begin{aligned}&\int_{t_0}^{t}\prod_{i\in\mathcal{R}_N}\exp\{\varsigma_{i(t_s)}T_{\mathrm{h}i}(\vartheta,t)-\varsigma_{\mathrm{s}i(t_s)}T_i(\vartheta,t)\}\gamma^2\|\boldsymbol{\omega}(\vartheta)\|^2\mathrm{d}\vartheta\\ \le&\gamma^2\int_{t_0}^{t}\prod_{i\in\mathcal{R}_N}\exp\{\varsigma_{i(t_s)}\tau_{\mathrm{h}}N_i(\theta,t)-\varsigma_{\mathrm{s}i(t_s)}T_i(\vartheta,t)\}\|\boldsymbol{\omega}(\vartheta)\|^2\mathrm{d}\vartheta\\ \le&\alpha\gamma^2\int_{t_0}^{t}\exp\{-\underline{\varsigma}_{\mathrm{u}}(t-\vartheta)\}\|\boldsymbol{\omega}(\vartheta)\|^2\mathrm{d}\vartheta.\end{aligned}\tag{20}$$

Let $t_0=0$. Combining inequalities (18)−(20), one can obtain that

$$\begin{aligned}&\int_{t_0}^{t}\exp\big(-\overline{\varsigma}_{\mathrm{s}}(t-\vartheta)\big)\|\boldsymbol{e}(\vartheta)\|^2\mathrm{d}\vartheta\\ \le&\alpha\gamma^2\int_{t_0}^{t}\exp\big(-\underline{\varsigma}_{\mathrm{u}}(t-\vartheta)\big)\|\boldsymbol{\omega}(\vartheta)\|^2\mathrm{d}\vartheta.\end{aligned}$$

Integrating two sides of the foregoing inequality for t from 0 to ∞, it holds that

$$\begin{aligned}&\int_0^{\infty}\int_0^{t}\exp\big(-\overline{\varsigma}_{\mathrm{s}}(t-\vartheta)\big)\|\boldsymbol{e}(\vartheta)\|^2\mathrm{d}\vartheta\mathrm{d}t\\ \le&\alpha\gamma^2\int_0^{\infty}\int_0^{t}\exp\big(-\underline{\varsigma}_{\mathrm{u}}(t-\vartheta)\big)\|\boldsymbol{\omega}(\vartheta)\|^2\mathrm{d}\vartheta\mathrm{d}t,\end{aligned}$$

which indicates that

$$\begin{aligned}&\int_0^{\infty}\|\boldsymbol{e}(\vartheta)\|^2\left(\int_{\vartheta}^{\infty}\exp\big(-\overline{\varsigma}_{\mathrm{s}}(t-\vartheta)\big)\mathrm{d}t\right)\mathrm{d}\vartheta\\ \le&\alpha\gamma^2\int_0^{\infty}\|\boldsymbol{\omega}(\vartheta)\|^2\left(\int_{\vartheta}^{\infty}\exp\big(-\underline{\varsigma}_{\mathrm{u}}(t-\vartheta)\big)\mathrm{d}t\right)\mathrm{d}\vartheta.\end{aligned}$$

It is noted that $\overline{\varsigma}_{\mathrm{s}}>0$ and $\underline{\varsigma}_{\mathrm{u}}>0$. One can further deduce that

$$\int_0^{\infty}\|\boldsymbol{e}(\vartheta)\|^2\mathrm{d}\vartheta\le\frac{\alpha\overline{\varsigma}_{\mathrm{s}}\gamma^2}{\underline{\varsigma}_{\mathrm{u}}}\int_0^{\infty}\|\boldsymbol{\omega}(\vartheta)\|^2\mathrm{d}\vartheta,$$

which demonstrates that tracking error system (5) achieves a non-weighted $\mathcal{H}_\infty$ performance as Eq. (11) according to Definition 2.

The following corollary can be derived based on Theorem 1 without considering interval partitioning or smooth interpolation. In this situation, the controller gain $\boldsymbol{K}_{\mathrm{e}i}(t)$ in control law (4) becomes a time-invariant matrix $\boldsymbol{K}_{\mathrm{e}i}$, $i\in\mathcal{R}_N$.

Corollary 1 Consider the switched linear system (2) with reference model (3). $\varsigma_i>0$ and $\mu_i>1$ are given constants for $i\in\mathcal{R}_N$. Supposing that there exist matrices $\boldsymbol{T}_i>0$ and $\boldsymbol{U}_i$ for $i\in\mathcal{R}_N$, $(i,j)\in\mathcal{R}_N\times\mathcal{R}_N$, $i\neq j$,

$$\begin{bmatrix}\mathrm{He}\{\boldsymbol{A}_i\boldsymbol{T}_i+\boldsymbol{B}_i\boldsymbol{U}_i\}+\varsigma_i\boldsymbol{T}_i & \boldsymbol{H}_i & \boldsymbol{T}_i\\ * & -\gamma^2\boldsymbol{I} & \boldsymbol{0}\\ * & \boldsymbol{0} & -\boldsymbol{I}\end{bmatrix}<0,$$

$$\boldsymbol{T}_j\le\mu_i\boldsymbol{T}_i,$$

for the MDDT switching law satisfying $\tau_{\mathrm{d}i}>\ln(\mu_i/\varsigma_i)$, $i\in\mathcal{R}_N$, system (5) is GUES with an $\mathcal{H}_\infty$ performance no greater than

$$\bar{\gamma}=\sqrt{-\frac{\bar{\varsigma}}{\bar{\varphi}}\prod_{i\in\mathcal{R}_N}\mu_i\gamma},$$

where $\bar{\varsigma}=\max_{i\in\mathcal{R}_N}(\varsigma_i)$ and $\bar{\varphi}=\max_{i\in\mathcal{R}_N}(\ln(\mu_i/\tau_{\mathrm{d}i})-\varsigma_i)$. In addition, the controller gains satisfy $\boldsymbol{K}_{\mathrm{e}i}\boldsymbol{T}_i=\boldsymbol{U}_i$, $\boldsymbol{A}_i+\boldsymbol{B}_i\boldsymbol{K}_{\mathrm{c}i}=\boldsymbol{A}_{\mathrm{r}}$, and $\boldsymbol{B}_i\boldsymbol{K}_{\mathrm{r}i}=\boldsymbol{B}_{\mathrm{r}}$, for $i\in\mathcal{R}_N$.

The proof is omitted here.

4 An example based on the XV-15 tilt-rotor aircraft

In this section, the XV-15 tilt-rotor aircraft is taken as an illustrative example to verify the effectiveness of the developed control method in Theorem 1.

Table 1 provides trimming results of each selected trimming point according to the conversion corridor, and the tilting process starts with $\beta_{\mathrm{M}}=0^\circ$ and $V=101.21$ ft/s (1 ft=0.3048 m). On this basis, the linearized Jacobian matrices of each trimming point can be obtained:

$$\boldsymbol{A}_1=\begin{bmatrix}-0.0282 & -0.0167 & 4.3608 & -32.1701\\ 0.0181 & -0.3791 & 101.0725 & 1.3874\\ -0.0421 & -0.6593 & 0 & 0\\ 0 & 0 & 1 & 0\end{bmatrix},$$

$$\boldsymbol{A}_2=\begin{bmatrix}-0.0387 & 0.0580 & -14.7603 & -32.0068\\ -0.0226 & -0.5043 & 134.1710 & -3.5221\\ 0.1309 & -0.9469 & 0 & 0\\ 0 & 0 & 1 & 0\end{bmatrix},$$

$$\boldsymbol{A}_3=\begin{bmatrix}-0.0554 & 0.1567 & -39.3071 & -31.3142\\ -0.0708 & -0.6455 & 164.1248 & -7.5007\\ 0.3873 & -1.2751 & 0 & 0\\ 0 & 0 & 1 & 0\end{bmatrix},$$

$$\boldsymbol{A}_4=\begin{bmatrix}-0.0672 & 0.1682 & -42.4852 & -31.4838\\ -0.0763 & -0.7647 & 198.0320 & -6.7533\\ 0.4153 & -1.5256 & 0 & 0\\ 0 & 0 & 1 & 0\end{bmatrix},$$

$$\boldsymbol{A}_5=\begin{bmatrix}-0.0879 & 0.1630 & -42.7192 & -31.7954\\ -0.0783 & -1.0004 & 266.6466 & -5.0877\\ 0.4103 & -2.0228 & 0 & 0\\ 0 & 0 & 1 & 0\end{bmatrix},$$

Table 1 Trimming results of the selected operating points

Mast angle	Air speed	System state				Control input		
β_{M}	V (ft/s)	u (ft/s)	w (ft/s)	q (rad/s)	θ (rad)	θ_{b} (rad)	θ_{a} (rad)	δ_{e} (rad)
0°	101.21	101.1160	−4.3608	0	−0.0431	0.5661	0	0.1011
12°	135.02	134.2099	14.7686	0	0.1096	0.4576	0	−0.1847
35°	168.78	164.1370	39.3157	0	0.2351	0.2658	0	−0.4413
52°	202.53	198.0255	42.4769	0	0.2113	0.2183	0	−0.3906
90°	270.04	266.6466	42.6757	0	0.1587	0.2432	0	−0.2821

1 ft=0.3048 m

$$\boldsymbol{B}_1=\begin{bmatrix}0 & 33.8880 & -0.1496\\ -59.9340 & 0 & -3.4695\\ 0 & 96.2554 & -42.8655\\ 0 & 0 & 0\end{bmatrix},$$

$$\boldsymbol{B}_2=\begin{bmatrix}12.4611 & 26.7040 & 0.6760\\ -58.6249 & 5.6761 & -6.1434\\ 0 & 78.0373 & -76.3834\\ 0 & 0 & 0\end{bmatrix},$$

$$\boldsymbol{B}_3=\begin{bmatrix}34.3774 & 12.5764 & 2.2496\\ -49.0960 & 8.8061 & -9.3919\\ 0 & 44.4269 & -118.2131\\ 0 & 0 & 0\end{bmatrix},$$

$$\boldsymbol{B}_4=\begin{bmatrix}47.2295 & 7.3092 & 2.9165\\ -36.8997 & 9.3554 & -13.5968\\ 0 & 34.6704 & -172.7129\\ 0 & 0 & 0\end{bmatrix},$$

$$\boldsymbol{B}_5=\begin{bmatrix}59.9333 & 0 & 3.9069\\ 0 & 12.0885 & -24.4113\\ 0 & 40.6470 & -316.5923\\ 0 & 0 & 0\end{bmatrix},$$

$$\boldsymbol{H}_1=\begin{bmatrix}0.1\\ 0.3\\ -0.5\\ 0\end{bmatrix},\boldsymbol{H}_2=\begin{bmatrix}0.2\\ 0.5\\ -0.2\\ 0\end{bmatrix},\boldsymbol{H}_3=\begin{bmatrix}-0.1\\ 0.2\\ 0.3\\ 0\end{bmatrix},$$

$$\boldsymbol{H}_4=\begin{bmatrix}-0.4\\ 0.2\\ -0.3\\ 0\end{bmatrix},\boldsymbol{H}_5=\begin{bmatrix}0.8\\ -0.2\\ -0.1\\ 0\end{bmatrix}.$$

The whole tilting process is represented by the five subsystems provided above.

The parameters of the reference system are given by

$$\boldsymbol{A}_{\mathrm{r}}=\begin{bmatrix}-0.0092 & -0.0011 & 0.1620 & -32.1996\\ 0.0039 & -0.1297 & 33.7596 & 0.1546\\ 0.0008 & -0.2525 & 0 & 0\\ 0 & 0 & 1 & 0\end{bmatrix},$$

$$\boldsymbol{B}_{\mathrm{r}}=\begin{bmatrix}1 & 0 & 0 & 0\end{bmatrix}^{\mathrm{T}},$$

and the reference input is selected as $r(t)=22\sin(0.1146t)$. External disturbance input, additionally, is considered as $\omega(t)=2\cos(0.53t)\mathrm{e}^{-0.05t}$.

Set $\varsigma_{\mathrm{u}1}=\varsigma_{\mathrm{u}2}=\varsigma_{\mathrm{u}3}=\varsigma_{\mathrm{u}4}=\varsigma_{\mathrm{u}5}=\varsigma_{\mathrm{s}1}=\varsigma_{\mathrm{s}2}=\varsigma_{\mathrm{s}3}=\varsigma_{\mathrm{s}4}=\varsigma_{\mathrm{s}5}=0.1$, $\tau_{\mathrm{h}}=0.8$, and $\tau_{\mathrm{l}1}=\tau_{\mathrm{l}2}=\tau_{\mathrm{l}3}=\tau_{\mathrm{l}4}=\tau_{\mathrm{l}5}=0.5$, and select $\gamma=1.1615$ and $L=1$.

Dealing with the conditions in Theorem 1, one can obtain

$$\boldsymbol{U}_{12}=\begin{bmatrix}-0.0187 & 0.0189 & 0.1197 & -0.0093\\ -0.0135 & -0.0189 & -0.0125 & 0.0010\\ -0.0237 & 0.1596 & -0.0070 & 0.0039\end{bmatrix},$$

$$\boldsymbol{U}_{21}=\begin{bmatrix}-0.4378 & -0.0469 & 0 & -0.0532\\ 0.1680 & -0.8188 & -0.0113 & 0.0147\\ 0.0839 & 0 & 0 & 0.0208\end{bmatrix},$$

$$\boldsymbol{U}_{22}=\begin{bmatrix}-0.0294 & -0.0083 & -0.0043 & -0.0044\\ -0.0086 & -0.0402 & -0.0085 & 0.0015\\ -0.0294 & 0.1139 & 0.0022 & 0.0021\end{bmatrix},$$

$$\boldsymbol{U}_{31}=\begin{bmatrix}-0.2846 & -0.1707 & 0 & -0.0750\\ 0.8171 & -1.5554 & -0.0187 & 0.1194\\ 0.1727 & 0 & 0 & 0.0482\end{bmatrix},$$

$$\boldsymbol{U}_{32}=\begin{bmatrix}-0.0344 & -0.0061 & -0.0715 & -0.0025\\ 0.0552 & -0.1752 & 0.0116 & 0.0099\\ -0.0241 & 0.0780 & 0.0119 & 0.0041\end{bmatrix},$$

$$\boldsymbol{U}_{41}=\begin{bmatrix}-0.3249 & -0.3610 & 0 & -0.1564\\ 2.0504 & -2.1442 & -0.0191 & 0.7170\\ 0.3292 & 0 & 0 & 0.1458\end{bmatrix},$$

$$\boldsymbol{U}_{42}=\begin{bmatrix}-0.0220 & 0.0246 & 0.2724 & -0.0009\\ 0.0238 & -0.1146 & 0.0280 & 0.0778\\ 0.0291 & 0.1694 & 0.0105 & 0.0167\end{bmatrix},$$

$$\boldsymbol{U}_{51}=\begin{bmatrix}-0.0093 & 0 & 0 & -0.0586\\ -1.0569 & 0.6317 & -0.0150 & 10.3686\\ -0.1717 & 0.5233 & 0 & 1.3322\end{bmatrix},$$

$$\boldsymbol{U}_{52}=\begin{bmatrix}-0.0053 & 0 & 0 & -0.0628\\ -0.7929 & 0.7681 & -0.0178 & 11.6953\\ -0.1403 & 0.5836 & 0 & 1.5020\end{bmatrix},$$

$$\boldsymbol{T}_{12}=\begin{bmatrix}0.4055&-0.0046&-0.0066&0.0059\\-0.0046&0.4006&0.0087&0.0037\\-0.0066&0.0087&0.1540&-0.0048\\0.0059&0.0037&-0.0048&0.0009\end{bmatrix},$$

$$\boldsymbol{T}_{21}=\begin{bmatrix}0.3948&0.0326&-0.0276&0.0037\\0.0326&0.3785&0.0102&-0.0024\\-0.0276&0.0102&0.4791&-0.0229\\0.0037&-0.0024&-0.0229&0.0018\end{bmatrix},$$

$$\boldsymbol{T}_{22}=\begin{bmatrix}0.3657&-0.0152&-0.0069&0.0041\\-0.0152&0.3656&-0.0002&0.0036\\-0.0069&-0.0002&0.0897&-0.0018\\0.0041&0.0036&-0.0018&0.0006\end{bmatrix},$$

$$\boldsymbol{T}_{31}=\begin{bmatrix}0.3730&0.0396&0.0414&-0.0053\\0.0396&0.3742&0.0299&-0.0053\\0.0414&0.0299&0.4231&-0.0261\\-0.0053&-0.0053&-0.0261&0.0029\end{bmatrix},$$

$$\boldsymbol{T}_{32}=\begin{bmatrix}0.3830&-0.0139&-0.0001&-0.0010\\-0.0139&0.3570&0.0097&-0.0012\\-0.0001&0.0097&0.0844&-0.0010\\-0.0010&-0.0012&-0.0010&0.0028\end{bmatrix},$$

$$\boldsymbol{T}_{41}=\begin{bmatrix}0.3513&0.0180&0.0360&-0.0092\\0.0180&0.3713&0.0321&-0.0075\\0.0360&0.0321&0.3775&-0.0526\\-0.0092&-0.0075&-0.0526&0.0170\end{bmatrix},$$

$$\boldsymbol{T}_{42}=\begin{bmatrix}0.3448&0.0072&-0.0032&-0.0012\\0.0072&0.3469&0.0199&-0.0014\\-0.0032&0.0199&0.2203&-0.0021\\-0.0012&-0.0014&-0.0021&0.0209\end{bmatrix},$$

$$\boldsymbol{T}_{51}=\begin{bmatrix}0.3813&0.0020&0.0252&-0.0472\\0.0020&0.3876&0.0182&-0.0144\\0.0252&0.0182&0.5221&-0.3385\\-0.0472&-0.0144&-0.3385&0.5064\end{bmatrix},$$

$$\boldsymbol{T}_{52}=\begin{bmatrix}0.3901&0.0011&0.0161&-0.0231\\0.0011&0.3949&0.0176&-0.0101\\0.0161&0.0176&0.5722&-0.3817\\-0.0231&-0.0101&-0.3817&0.5780\end{bmatrix}.$$

Additionally, $\boldsymbol{U}_i(t)$ and $\boldsymbol{T}_i(t)$ can be derived from Eqs. (12) and (13), respectively. Meanwhile, the controller gain matrices can be deduced by $\boldsymbol{K}_{ei}(t)=\boldsymbol{U}_i(t)\boldsymbol{T}_i^{-1}(t)$, $\boldsymbol{A}_i+\boldsymbol{B}_i\boldsymbol{K}_{ci}=\boldsymbol{A}_{\mathrm{r}}$, and $\boldsymbol{B}_i\boldsymbol{K}_{ri}=\boldsymbol{B}_{\mathrm{r}}$.

Set $\gamma=1.0595$, $\varsigma_1=\varsigma_2=\varsigma_3=\varsigma_4=\varsigma_5=0.1$, and $\mu=1.3$, and deal with the conditions in Corollary 1. By similar manipulation, $\boldsymbol{K}_{ci}$ and $\boldsymbol{K}_{ri}$ share the same values in Theorem 1, and $\boldsymbol{K}_{ei}$ for $i\in\mathcal{R}_N$ are

$$\boldsymbol{K}_{\mathrm{e1}}=\begin{bmatrix}0.0902&0.1170&0.5060&-8.7093\\-0.0563&-0.0607&-0.0344&1.4909\\-0.1083&0.3619&0.0450&3.7505\end{bmatrix},$$

$$\boldsymbol{K}_{\mathrm{e2}}=\begin{bmatrix}0.0054&0.0544&-0.2046&-7.8495\\-0.0697&-0.1480&-0.0290&3.5646\\-0.0947&0.2836&0.0674&2.4529\end{bmatrix},$$

$$\boldsymbol{K}_{\mathrm{e3}}=\begin{bmatrix}-0.0934&-0.0015&-0.8613&-1.2124\\0.1356&-0.4803&0.2334&3.4144\\-0.0508&0.2182&0.1343&1.5734\end{bmatrix},$$

$$\boldsymbol{K}_{\mathrm{e4}}=\begin{bmatrix}-0.0520&0.0014&1.2362&0.0770\\0.0906&-0.3276&0.1935&3.7293\\0.0773&0.4894&0.0127&0.8406\end{bmatrix},$$

$$\boldsymbol{K}_{\mathrm{e5}}=\begin{bmatrix}-0.0197&0.0009&-0.1295&-0.1950\\-0.8890&1.7971&24.0109&36.0877\\-0.2151&1.4604&3.0490&4.6291\end{bmatrix}.$$

The total runtime of tilting is 15 s, and the selected switching signal is displayed in Fig. 1, which depends on the intervals between adjoining trimming points. The MDDT constraints of Theorem 1 and Corollary 1 are both satisfied.

The comparison of Theorem 1 and Corollary 1 is displayed in one figure to highlight the difference. Figs. 2–5 track performances of forward speed u, longitudinal speed w, pitch rate q, and pitch angle θ, respectively. Both control schemes of Theorem 1 and Corollary 1 are capable of accomplishing state tracking and control. However, the control scheme of Theorem 1 has better tracking control performance than the scheme of Corollary 1, particularly at switching instants.

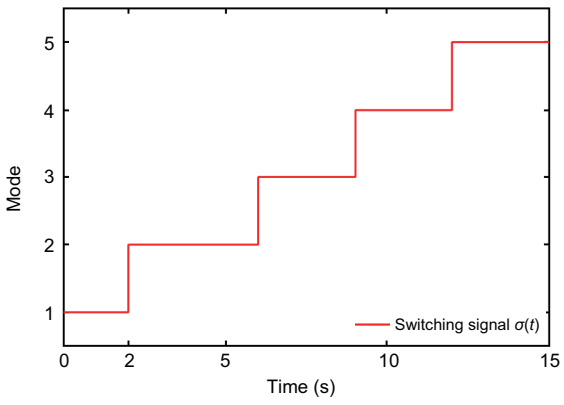

Fig. 1 Switching signal $\boldsymbol{\sigma(t)}$

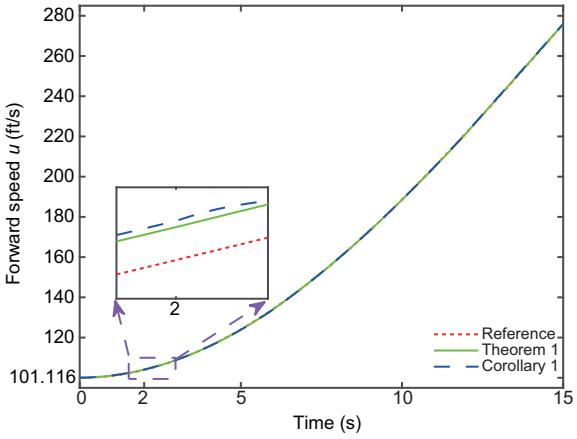

Fig. 2 Forward speed u (1 ft=0.3048 m)

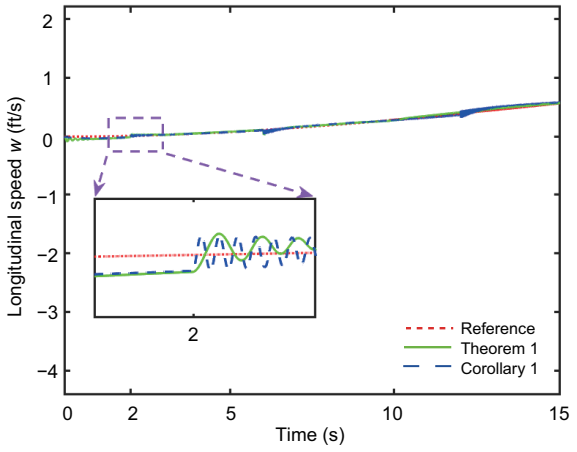

Fig. 3 Longitudinal speed w (1 ft=0.3048 m)

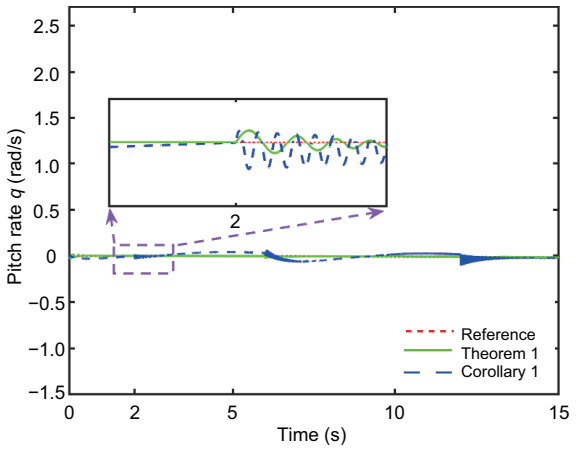

Fig. 4 Pitch rate q

5 Conclusions

In this paper, a switched linear modeling method is provided for the conversion mode of a tilt-rotor aircraft. An $\mathcal{H}_\infty$ state-tracking control law is designed that transforms the nonlinear control issue of conversion mode into a stabilization problem of the switched linear system. Moreover, the linear interpolation and interval partitioning methods are further developed to restrain the abrupt controller bumps at switching instants. Finally, the effectiveness and advantages of the proposed control scheme are validated by using the XV-15 aircraft as an example. It is worth mentioning that the linearization process leads to inevitable error between the switched linear model and the original nonlinear model, which has a certain impact on the performance of the system. To deal with this issue, a switched Takagi–Sugeno fuzzy modeling method can be further pursued to improve the accuracy of modeling in future studies.

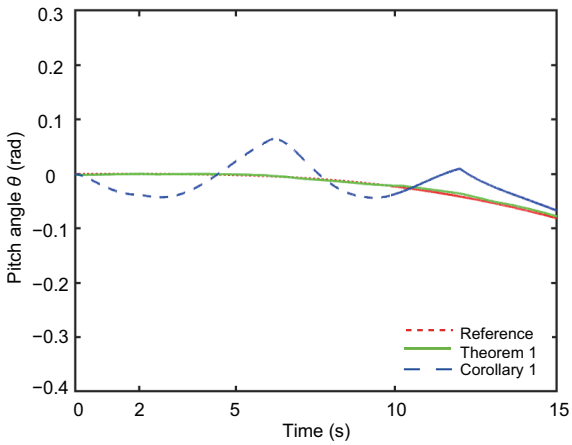

Fig. 5 Pitch angle θ

Contributors

Shuang SHI designed the research. Kebi LUO processed the data and drafted the paper. Shuang SHI helped organize the paper. Cong PENG revised and finalized the paper.

Compliance with ethics guidelines

Kebi LUO, Shuang SHI, and Cong PENG declare that they have no conflict of interest.

Data availability

The data that support the findings of this study are available from the corresponding author upon reasonable request.

References

Abà A, Barra F, Capone P, et al., 2020. Mathematical modelling of gimballed tilt-rotors for real-time flight simulation. *Aerospace*, 7(9):124. https://doi.org/10.3390/aerospace7090124

Allerhand LI, Shaked U, 2011. Robust stability and stabilization of linear switched systems with dwell time. *IEEE Trans Autom Contr*, 56(2):381-386. https://doi.org/10.1109/TAC.2010.2097351

Barra F, Godio S, Guglieri G, et al., 2019. Implementation of a comprehensive mathematical model for tilt-rotor real-time flight simulation. 45th European Rotorcraft Forum, Article 0020. https://doi.org/10.21256/zhaw-19753

Chen C, Zhang JY, Zhang DB, et al., 2017. Control and flight test of a tilt-rotor unmanned aerial vehicle. *Int J Adv Robot Syst*, 14(1). https://doi.org/10.1177/1729881416678141

Daafouz J, Geromel JC, Deaecto GS, 2012. A simple approach for switched control design with control bumps limitation. *Syst Contr Lett*, 61(12):1215-1220. https://doi.org/10.1016/j.sysconle.2012.09.001

Fei ZY, Chen WZ, Zhao XD, et al., 2023. Stabilization of switched linear neutral systems with time-scheduled feedback control strategy. *IEEE Trans Autom Contr*, 68(2):1093-1100. https://doi.org/10.1109/TAC.2022.3146708

Harendra PB, Joglekar MJ, Gaffey TM, et al., 1973. V/STOL Tilt Rotor Study. Volume 5: a Mathematical Model for Real Time Flight Simulation of the Bell Model 301 Tilt Rotor Research Aircraft. Technical Report No. BELL-301-099-001-VOL-5, Bell Helicopter Co., Fort Worth, TX, USA.

Hou LL, Ma X, Sun HN, 2022. Stabilization of switched linear systems under asynchronous switching subject to admissible edge-dependent average dwell time. *Front Inform Technol Electron Eng*, 23(5):810-822. https://doi.org/10.1631/FITEE.2000698

Kleinhesselink KM, 2007. Stability and control modeling of tiltrotor aircraft. MS Thesis, University of Maryland, College Park, MD, USA.

Kong ZW, Lu Q, 2018. Mathematical modeling and modal switching control of a novel tiltrotor UAV. *J Robot*, 2018:8641731. https://doi.org/10.1155/2018/8641731

Li YL, Wang HQ, Zhao XD, et al., 2022. Event-triggered adaptive tracking control for uncertain fractional-order nonstrict-feedback nonlinear systems via command filtering. *Int J Robust Nonl Contr*, 32(14):7987-8011. https://doi.org/10.1002/rnc.6255

Li Z, Xia P, 2018. Aeroelastic modelling and stability analysis of tiltrotor aircraft in conversion flight. *Aeronaut J*, 122(1256):1606-1629. https://doi.org/10.1017/aer.2018.93

Maisel MD, Giulianetti DJ, Dugan DC, 2000. The History of the XV-15 Tilt Rotor Research Aircraft from Concept to Flight. NASA, Washington, DC, USA. https://history.nasa.gov/monograph17.pdf

Roy S, Baldi S, Ioannou PA, 2022. An adaptive control framework for underactuated switched Euler–Lagrange systems. *IEEE Trans Autom Contr*, 67(8):4202-4209. https://doi.org/10.1109/TAC.2021.3108507

Rysdyk R, Calise AJ, 2005. Robust nonlinear adaptive flight control for consistent handling qualities. *IEEE Trans Contr Syst Technol*, 13(6):896-910. https://doi.org/10.1109/TCST.2005.854345

Rysdyk RT, Calise AJ, 1999. Adaptive model inversion flight control for tilt-rotor aircraft. *J Guid Contr Dyn*, 22(3):402-407. https://doi.org/10.2514/2.4411

Shi S, Fei ZY, Zhao XD, 2021. Time-scheduled observer design for switched linear systems with unknown inputs. *Sci China Inform Sci*, 65(7):179204. https://doi.org/10.1007/s11432-020-3143-7

Tang FH, Niu B, Zong GD, et al., 2022. Periodic event-triggered adaptive tracking control design for nonlinear discrete-time systems via reinforcement learning. *Neur Netw*, 154:43-55. https://doi.org/10.1016/j.neunet.2022.06.039

Thompson TH, 1990. The Bell Helicopter XV-3 and XV-15 experimental aircraft—lessons learned. Aircraft Design, Systems and Operations Conf. https://doi.org/10.2514/6.1990-3265

Wang XH, Cai LL, 2015. Mathematical modeling and control of a tilt-rotor aircraft. *Aerosp Sci Technol*, 47:473-492. https://doi.org/10.1016/j.ast.2015.10.012

Wang YE, Sun XM, Mazenc F, 2016. Stability of switched nonlinear systems with delay and disturbance. *Automatica*, 69:78-86. https://doi.org/10.1016/j.automatica.2016.02.015

Xiang WM, 2015. On equivalence of two stability criteria for continuous-time switched systems with dwell time constraint. *Automatica*, 54:36-40. https://doi.org/10.1016/j.automatica.2015.01.033

Yang D, Zhao J, 2019. $\mathcal{H}_\infty$ bumpless transfer for switched LPV systems and its application. *Int J Contr*, 92(8):1945-1958. https://doi.org/10.1080/00207179.2017.1421774

Ye J, Roy S, Godjevac M, et al., 2021. A switching control perspective on the offshore construction scenario of heavy-lift vessels. *IEEE Trans Contr Syst Technol*, 29(1):470-477. https://doi.org/10.1109/TCST.2020.2978446

Yuan S, Zhang LX, De Schutter B, et al., 2018. A novel Lyapunov function for a non-weighted $\mathcal{L}_2$ gain of asynchronously switched linear systems. *Automatica*, 87:310-317. https://doi.org/10.1016/j.automatica.2017.10.018

Zhao H, Zong GD, Zhao XD, et al., 2023. Hierarchical sliding-mode surface-based adaptive critic tracking control for nonlinear multiplayer zero-sum games via generalized fuzzy hyperbolic models. *IEEE Trans Fuzzy Syst*, 31(11):4010-4023. https://doi.org/10.1109/TFUZZ.2023.3273566

Zhao XD, Zhang LX, Shi P, et al., 2012. Stability and stabilization of switched linear systems with mode-dependent average dwell time. *IEEE Trans Autom Contr*, 57(7):1809-1815. https://doi.org/10.1109/TAC.2011.2178629

Zhao Y, Zhao J, 2020. $\mathcal{H}_\infty$ reliable bumpless transfer control for switched systems with state and rate constraints. *IEEE Trans Syst Man Cybern Syst*, 50(19):3925-3935. https://doi.org/10.1109/TSMC.2018.2871335

Zhao Y, Zhao J, Fu J, et al., 2020. Rate bumpless transfer control for switched linear systems with stability and its application to aero-engine control design. *IEEE Trans Ind Electron*, 67(6):4900-4910. https://doi.org/10.1109/TIE.2019.2931222